Investigations of mechanism, surface species and support effects in CO hydrogenation over Rh

Max Schumann [a], Jan-Dierk Grunwaldt [b,c], Anker D. Jensen [a], Jakob M. Christensen [a,*]

[a] *Department of Chemical and Biochemical Engineering, Technical University of Denmark, 2800 Kgs. Lyngby, Denmark*
[b] *Institute for Chemical Technology and Polymer Chemistry (ITCP), Karlsruhe Institute of Technology, 76131 Karlsruhe, Germany*
[c] *Institute of Catalysis Research and Technology (IKFT), Karlsruhe Institute of Technology, 76344 Eggenstein-Leopoldshafen, Germany*

ARTICLE INFO

ABSTRACT

The Rh-catalyzed CO hydrogenation to hydrocarbons and C_2-oxygenates over Rh/ZrO_2 and Rh/SiO_2 was studied. Catalytic reaction tests show a support effect with a faster steady state reaction rate over Rh/ZrO_2 compared to Rh/SiO_2. Temperature programmed hydrogenation (TPH) experiments reveal that the CO dissociation on the metal surface is rate limiting, and the support effect thus accelerates the CO dissociation on the metal. Combined TPH and diffuse reflectance infrared Fourier transform spectroscopy (DRIFTS) studies after low-temperature CO pre-adsorption reveal a H-assisted C-O bond breakage through CH_3O species on the Rh surface. Transient measurements indicate that this mechanism is also likely to be in operation during the steady state reaction at higher temperatures, although here the methoxide is too short-lived to be detected at steady state. This hydrogen-assisted CO activation can help to explain that previous studies have observed an inverse H/D isotope effect for Rh despite CO dissociation being the rate limiting step. TPH studies show that both CO pre-adsorption at 30 ℃ and CO/H_2 exposure at 250 ℃ lead to so high CO coverages that it restricts the CO activation, which only starts once part of the CO has desorbed. The near-complete CO coverage on the working Rh surface is restricting the rate, but is essential for the selectivity towards oxygenates. Studies of acetaldehyde conversion in various atmospheres over Rh/SiO_2 and Rh/ZrO_2 catalysts show that acetaldehyde decomposes over a bare Rh surface with a rate that greatly exceeds the oxygenate formation rate in CO hydrogenation. In the presence of CO the acetaldehyde decomposition is strongly inhibited. The high CO coverage on the surface of the working Rh catalysts thus prevents oxygenate decomposition and is therefore essential for the ability to produce oxygenated products. The reaction temperature is observed to play a role for the establishment of the high coverage. During exposure to CO/H_2 at reaction temperatures (>200 ℃) an activated process occurs whereby both the stability and coverage of the CO adlayer increases. This activated stabilization of the CO adlayer shifts the CO activation up in temperature in a subsequent TPH. The results contribute to a fundamental understanding of the reaction mechanism and support effects in the Rh-catalyzed CO hydrogenation, which can assist the formulation of improved Rh-based catalysts. The results, such as the identification of a H-assisted mechanism of CO hydrogenenation via methoxide, could also be of general relevance for the understanding of CO hydrogenation over other metals.

1. Introduction

Rhodium-based catalysts are active for syngas conversion and are of particular interest due to their superior selectivity towards C_2-oxygenates [1,2]. Rh catalysts could therefore be of potential use for the synthesis of fuel additives or value-added platform molecules from sustainably derived syngas [3]. However, the unfavorably low intrinsic activity of Rh-based catalysts and the high cost of the metal are disadvantageous for their application at industrial scale. Previous studies [4–7] have identified strong support and promoter effects that result in a markedly increased catalytic activity for syngas conversion and substantial changes in the product distribution. Although significant improvements in the catalytic activity have been obtained by using favorable combinations of support and promoting additives [8,9], the understanding of support/promoter effects is still insufficient to enable catalysts of an industrially acceptable activity. Despite a widely accepted overall reaction mechanism being in place [10–12], involving CO dissociation and subsequent CO insertion forming CH_xCO species

---

that lead to oxygenates, several aspects of the reaction mechanism remain ambiguous [1,13,14]. Importantly, the nature of CO dissociation, the most likely rate determining step, is not yet clarified. Experiments show that direct CO dissociation is possible on Rh [10], but observations have also revealed the existence of an (inverse) H/D isotope effect [15,16], which suggests H to be involved in the rate limiting reaction step. Studies employing density functional theory (DFT) have suggested a (potentially faster) direct dissociation of CO over stepped Rh surfaces [11], and H-assisted pathways for CO dissociation that are especially important over planar Rh terrace sites [12,17,18]. The extent of involvement of hydrogen in the rate limiting step and the nature of the possible hydrogenated CO species that facilitate C-O bond breakage thus remain unclear. When it comes to the product distribution it is also insufficiently understood how the catalytic reaction can yield any C_2-oxygenates, when experimental studies on Rh single crystals [19–21] or supported Rh catalysts [22,23] as well as theoretical calculations [24,25] consistently indicate a facile decomposition of the oxygenates on Rh even at sub-ambient temperatures.

An understanding of how activity is enhanced by support/promoter effects is intrinsically linked to a mechanistic understanding, as support/promoter effects must impact the rate limiting step(s) in the mechanism. Currently it is not yet clear whether the support/promoter effect is primarily via the metal through a modification of the electronic properties of Rh [26], through local interaction between support-derived species and CO to facilitate CO dissociation [27], or through opening of new bifunctional reaction pathways – for example via acetate species that include oxygen from the support/promoter [28–30]. When investigated together the reaction mechanism and the support effects may thus help to illuminate each other and this is the purpose of the present study.

In this study silica-supported Rh is compared to Rh on zirconia, as ZrO_2 is a support which is known to exert a marked promotional support effect on rhodium [31–33]. Steady state experiments and temperature programmed hydrogenation experiments coupled with infrared spectroscopy and mass spectrometry analysis of the reactor effluent gases are employed to elucidate the reaction mechanism and its interplay with the support.

2. Experimental section

2.1. Catalyst preparation

The catalysts were prepared by wet impregnation where the desired amount of $Rh(NO_3)_3$ (Sigma Aldrich, ca. 36 wt% Rh) was dissolved in demineralized water and subsequently impregnated onto pre-calcined (1 h in flowing air at 400 °C for silica and 550 °C for zirconia, rate: 10 °C/min) and sieve-fractioned (150 – 300 µm) SiO_2 (Saint Gobain SS61138, 252 m^2/g) or monoclinic m–ZrO_2 (Saint Gobain SZ 31163, 57.2 m^2/g) support material. Nominal Rh loadings were 1 wt% on ZrO_2 as well as 1 and 5.5 wt% on SiO_2. For Rh/SiO_2 the mechanistic analyses focused on the more active 5.5 wt% sample, which gave stronger product signals during TPH.

After impregnation, residual water was removed under reduced pressure in a rotary evaporator. The dried, yellowish-colored catalyst was calcined in flowing air at 400 °C when using silica, and at 550 °C in the case of zirconia (ramp rate: 5 °C/min, 60 min isothermal period). Before any experiments, the catalysts were reduced in hydrogen *in situ* at 400 °C for 120 min (ramp rate: 5 °C/min).

2.2. Catalyst characterization and reaction testing

2.2.1. H_2-Temperature programmed desorption (TPD) characterization

H_2-TPD measurements were carried out on a Quantachrome Autosorb iQ$_2$ chemisorption station connected to a Hiden Analytical QGA MS. Pre-reduced 1 % Rh/ZrO_2 was ramped in H_2 to 400 °C (rate: 5 °C/min, 120 min), cooled down to 200 °C, evacuated for 1 h, set under H_2 flow for 1 h, switched to He atmosphere to purge physisorbed hydrogen and then cooled down in He to 30 °C. The sample was kept in flowing He for 30 min and then heated to 700 °C with 5 °C/min. The amount of chemisorbed hydrogen was determined from integration of the hydrogen desorption signal. A 5 vol% H_2/He (AGA) gas mixture was used to calibrate the MS signal for H_2.

2.2.2. Tests of the catalytic performance

Catalytic performance was evaluated using a high-pressure set-up with product analysis by gas chromatography (GC) described elsewhere [34]. In brief, a quartz tube (i.d.: 8 mm, o.d.: 10 mm) held the catalyst (bed length ca. 2 to 6 cm) which was fixed between wads of quartz wool. The void volume was filled by quartz glass rods. The quartz tube was placed inside a TP347 stainless steel pressure shell which always had nitrogen pressure (dosed via Brooks 5866 mass flow pressure controllers) identical to the one within the quartz tube to avoid pressure gradients across the quartz tube. The ensemble of reactor tube and pressure shell was placed inside an Entech tube oven with the catalyst within the isothermal zone of the oven. The feed gases, N_2 (Air Liquide), H_2 (Air Liquide, N5.0), CO (Air Liquide, N3.7), and 1598 ppm acetaldehyde in nitrogen (AGA, Linde), were supplied from pressurized gas cylinders via Brooks 5850S mass flow controllers and mixed before entering the reactor tube. All post-reactor gas lines were heat traced at 135 °C. Downstream of the set-up, the pressure was relieved via a pneumatically operated pressure reduction valve (Baumann 5115S) and the gas flow was directed to a GC (6890 N, Agilent Technologies). The GC was equipped with flame ionization and thermal conductivity detectors and used He as carrier gas. Calibration details and detected compounds are listed in the supporting information.

Unless stated otherwise, the total CO/H_2 (volumetric ratio: V/V = 1/2) reactant pressure was set to 20 bar, reaction temperature was 250 °C and 225 °C for Rh/SiO_2 and Rh/ZrO_2 respectively, the flow rate of CO/H_2 was 40 NmL min^{-1} with a flow rate to catalyst mass ratio (F/W) of 4000 NmL min^{-1} g$_{Rh}^{-1}$ and during catalytic reaction tests the samples were held on stream for at least 8 h. Post-catalysis microscopy analysis by the method described elsewhere [37] showed that the size distribution for the spent catalyst had a major overlap with the distribution for the freshly reduced sample, which suggests that sintering is limited under these reaction conditions. Additionally, re-calcination and re-reduction of a spent 1 % Rh/SiO_2 catalyst restored the original performance. On this basis it is concluded that the present results are not significantly affected by sintering.

2.2.3. Conversion of acetaldehyde in different reaction atmospheres

The conversion of acetaldehyde when directed over supported Rh catalysts under typical reaction temperature and pressure conditions was investigated. Here, a gas mixture containing 1598 ppm acetaldehyde in nitrogen (AcH/N_2) was either co-fed with CO/H_2, with pure H_2, or passed over the catalyst alone. To retain the same partial pressure levels of the CO/H_2 reactants (20 bar) when adding AcH/N_2 to CO/H_2, the total pressure was increased to 27 bar under these testing conditions. While directing AcH/N_2 or AcH/N_2/H_2 over the catalyst, the total pressure was set to 20 bar. Co-feeding the AcH/N_2 gas mixture to H_2 or CO/H_2 leads to a dilution of the original AcH concentration (1598 ppm). An overview of the applied reaction parameters and the prevailing concentration levels of co-fed AcH is provided in Table 1.

2.2.4. DRIFTS experiments

Transient response experiments, monitoring changes to surface species when switching from CO/H_2 to H_2 reaction atmosphere,

Table 1
Overview of reaction gas compositions when investigating the catalytic conversion of co-fed acetaldehyde (1598 ppm AcH in N_2) in different reaction atmospheres. Catalyst samples used: 1 % Rh/SiO_2 and 1 % Rh/ZrO_2, catalyst mass: 1.00 g, reaction temperature: 250 °C for 1 % Rh/SiO_2 and 225 °C for 1 % Rh/ZrO_2.

Reaction test (Panel in Fig. 4)	Reaction atmosphere	Atmosphere composition [V: V]	Total flow rate [NmL min^{-1}]	Total pressure [bar]	AcH concentration [ppmv]
0	CO + H_2	1: 2	40	20	–
1 (A)	AcH/N_2	1	40	20	1598
2 (B)	AcH/N_2 + H_2	1: 2	40	20	533 [a]
3 (C)	AcH/N_2 + CO + H_2	1: 1: 2	53.3	27	399 [a]

[a] These conditions are selected to yield the same molar feed flow of AcH.

were conducted on a DRIFTS set-up described previously in more detail [35]. In brief, experiments were carried out in a Praying Mantis™ diffuse reflection optics unit equipped with a high pressure cell (Harrick Scientific Products). Spectra were collected with a Nicolet iS50 FTIR spectrometer with a liquid-N_2 cooled MCT detector and averaged over 64 measurements with 4 cm^{-1} resolution. Effluent gases were monitored by on-line mass spectrometry (MS) using a Hiden Analytical HPR-20 EGA mass spectrometer. Four different types of experiments were conducted. For each experiment samples were reduced *in situ* (2 h in H_2 at 400 °C, rate: 5 °C/min). The total flow rate for all flows was 40 mL min^{-1} and the pressure was 1 bar unless specified otherwise. Temperature values refer to both catalysts, 5.5 % Rh/SiO_2 and 1 % Rh/ZrO_2, unless specified otherwise. The loaded catalyst mass was ca. 40 mg for Rh/SiO_2 and ca. 120 mg for Rh/ZrO_2; differing due to the different densities of the oxides.

2.2.5. Transient response experiments: Changing atmosphere from CO/H_2 to H_2

In a first experiment, the pre-reduced catalyst sample was ramped to 250 °C in H_2 atmosphere (a background spectrum was recorded under these conditions) and the atmosphere was then switched to CO/H_2 (V/V = 1/2). The pressure was set to 16 bar by closing the needle valve. DRIFTS spectra were continuously collected and the sample was allowed to reach a steady state adsorbate coverage. The CO feed was then stopped and the sample was kept in a pure H_2 flow at 13 bar and 250 °C for ca. 4 h.

2.2.6. TPH after pretreatment under catalytic CO/H_2 reaction conditions

In a second experiment, the catalyst was pre-reduced and a background spectrum was recorded in H_2 atmosphere at 30 °C. At atmospheric pressure the catalyst sample was then ramped to 250 °C in H_2 atmosphere and the atmosphere was switched to CO/H_2/Ar (V/V = 1/2/9) in which the catalyst was held for ca. 1 h. The pressure was increased to 16 bar and the catalyst held under these conditions for 2 h; allowing the sample to reach a steady state coverage as monitored by the IR signals. The pressure was then released and the sample rapidly cooled down to 30 °C in reaction atmosphere. Reactant gases were purged by a He flow for 30 min at 30 °C, and the sample was then kept in a H_2 flow for 45 min. The sample was subjected to a TPH by heating to 500 °C with a rate of 5 °C/min in flowing H_2.

2.2.7. TPH after CO pre-adsorption at low temperature

In a third experiment, the catalyst was pre-reduced and a background spectrum was recorded at 30 °C in a H_2 atmosphere. The catalyst sample was then, at atmospheric pressure, exposed to a 9.5 % CO/Ar flow at 30 °C for 30 min to adsorb CO. Afterwards, residual CO was purged by a He flow for 30 min and the sample was then kept under a H_2 flow for 45 min. The sample was subjected to a TPH by heating to 500 °C with a rate of 5 °C/min in flowing H_2.

2.2.8. Transient response experiments: Changing atmosphere from CO to H_2

In a fourth experiment, the pre-reduced catalyst sample was ramped in H_2 to 250 °C for 5.5 % Rh/SiO_2, or 225 °C for Rh/ZrO_2. A background spectrum was recorded under these conditions and the atmosphere was then switched to a flow of pure CO. The pressure was increased to 17 bar by closing the needle valve. After 20 min of CO flow under these conditions, the CO atmosphere was displaced by a He flow that was maintained until absorption bands ascribed to gaseous CO could no longer be detected. The He flow was then switched to H_2 flow and the sample was kept in flowing H_2 at 11.5 bar until no further changes in the spectra were detected.

3. Results and discussion

3.1. Characterization of Rh particle sizes

The CO hydrogenation over Rh is highly structure sensitive for smaller (<ca. 5 nm) particles [36,37], and knowledge of the particle size is therefore critical for studies of this reaction. Table 2 shows the average particle sizes for the investigated samples. For Rh/SiO_2 catalysts the particle sizes were extracted from statistical analysis of TEM images as described in a previous study [37]. For Rh/ZrO_2 the hydrogen chemisorption capacity measured by temperature programmed desorption (TPD) of H_2 was used to estimate the Rh particle size. Ligthart et al. [38] have shown a good agreement between particle size estimates from H_2 chemisorption and TEM, which suggests that chemisorption results should be reasonably representative. TPD for the 1 % Rh/ZrO_2 catalyst yielded a molar H–uptake of H/Rh_{total} = 0.96. This value cannot be directly equated to a dispersion because the adsorption stoichiometry is highly size dependent for small particles [37,39,40]. Thus, the Rh particle size for 1 % Rh/ZrO_2 was estimated on the basis of the obtained H/Rh_{total} value and the relation between H/Rh_{total} and the particle size found by TEM for Rh/SiO_2 catalysts [37] (Fig. S1).

3.2. Catalytic reaction tests – Support effects

Fig. 1 shows an Arrhenius plot for the rate of CO conversion under differential conditions (<3% CO conversion) on 1 wt%

Table 2
Number-weighted, mean particle diameters and H/Rh_{total} values for the Rh catalysts. Particle diameters were calculated from statistical analysis of TEM images and estimation of the metal dispersion was derived from H_2-TPD.

Catalyst sample	Particle diameter [nm]	H/Rh_{total}
1 % Rh/SiO_2	1.7[a]	1.38 [a]
5.5 % Rh/SiO_2	3.5[a]	0.71 [a]
1 % Rh/ZrO_2	∼ 2.7[b]	0.96

[a] Number based average particle diameter from TEM measurements from Schumann et al.[37].
[b] Estimated from the relation between hydrogen uptake and the TEM particle size reported by Schumann et al. [37] (Fig. S1).
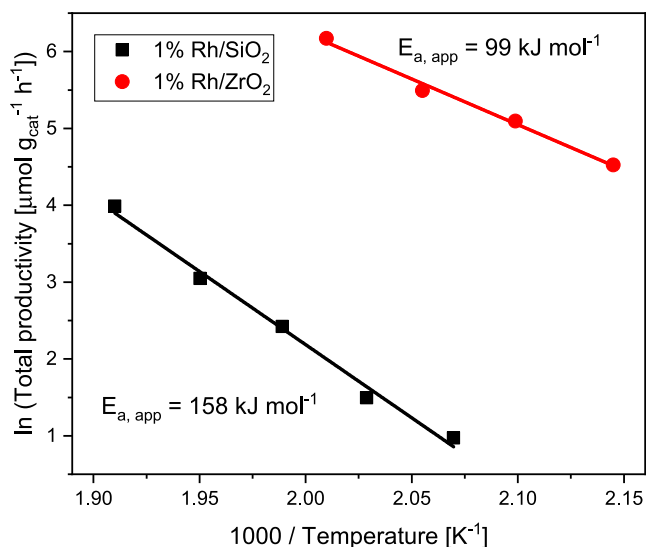
Fig. 1. Arrhenius plot for the rate of CO hydrogenation over 1 wt% Rh supported on SiO$_2$ (squares) or ZrO$_2$ (circles). Reaction conditions: 20 bar of CO/H$_2$ (V/V = 1/2), catalyst mass = 1.00 g for 1 % Rh/SiO$_2$ and 2.00 g for 1 % Rh/ZrO$_2$, F/W = 4000 NmL min^{-1} g$_{Rh}^{-1}$. Detailed information about selectivities and conversions are summarized in Tables S1-S2.

Rh/ZrO$_2$ and 1 wt% Rh/SiO$_2$ and illustrates the strong support effect. Fig. 2 compares the catalytic performance of the silica and zirconia supported Rh catalysts and illustrates that the support not only impacts the catalytic activity but also the selectivity. Here, Rh/ZrO$_2$ is more active toward CO hydrogenation than Rh/SiO$_2$ regardless of the studied Rh particle size (see diameters in Table 2). Structure sensitivity is therefore not the main reason for the activity differences. For further studies, 225 °C was selected as the reaction temperature for Rh/ZrO$_2$ because the formation of liquid products from the more active ZrO$_2$-supported catalyst created practical difficulties at higher temperatures. The Rh/SiO$_2$ catalysts were tested at 250 °C, because the low productivity of the 1 wt% catalyst Rh/SiO$_2$ led to significant uncertainties at lower temperatures.

Fig. 2 illustrates that the selectivity is also impacted by the support effect. For Rh/ZrO$_2$ the selectivity towards the desirable C$_2$-oxygenate products is lower compared to Rh/SiO$_2$. Moreover, the relative distribution between acetaldehyde and ethanol is strongly dependent upon the choice of support. Acetaldehyde is the dominant oxygenate for Rh/SiO$_2$, whereas ethanol (EtOH) is the dominant oxygenate for Rh/ZrO$_2$. A similar shift towards ethanol was also reported for rare earth oxide supports [7]. The catalytic results thus indicate that the support effect is an enhancement of the rate determining reaction step and an altered hydrogenation capability that shifts the oxygenate product from acetaldehyde towards ethanol.

3.3. Catalytic reaction tests – Further conversion of acetaldehyde

The conversion of acetaldehyde was evaluated under various reaction conditions in order to understand why oxygenated products such as acetaldehyde and ethanol are formed in CO hydrogenation despite the fact that decomposition of such oxygenates is reportedly [19,41] facile on Rh surfaces. Fig. 3 illustrates the stability of acetaldehyde when an AcH/N$_2$ stream is directed over Rh/SiO$_2$ (Fig. 3A) or Rh/ZrO$_2$ (Fig. 3B) at temperature and pressure relevant for the CO hydrogenation reaction. For both catalysts, acetaldehyde decomposes readily when brought into contact with the bare Rh surface (i.e. in the absence of added CO/H$_2$). The resulting CO and CH$_4$ constitute the major decomposition products, which is in line with previous reports [19] of acetaldehyde decomposition via decarbonylation on rhodium. For 1 % Rh/SiO$_2$, complete decomposition of acetaldehyde into an approximately equimolar CO/CH$_4$ mixture is observed already after short time on stream (<3h). Given the full conversion of acetaldehyde this experiment only gives a lower limit for the decarbonylation rate of at least 169 µmol g$_{cat}^{-1}$.h^{-1}. By comparison, the CO hydrogenation rate for 1 % Rh/SiO$_2$ at the same conditions (Fig. 2) is around 45 µmol g$_{cat}^{-1}$.h^{-1}, so the aldehyde decomposition would be fast enough to remove all formed oxygenated products on a bare rhodium surface. For 1 % Rh/ZrO$_2$ a pronounced transient change can be seen in the product distribution during the initial period of aldehyde exposure. Initially, only CH$_4$ escapes suggesting that the CO from decarbonylation is retained on the rhodium surface. The CO selectivity in the effluent gas then gradually approaches 50 % as expected from complete decarbonylation. That CO begins to escape indicates that the Rh surface is becoming saturated with adsorbed CO. When approaching surface saturation by CO the aldehyde conversion drops from 100 %, and acetaldehyde also begins to
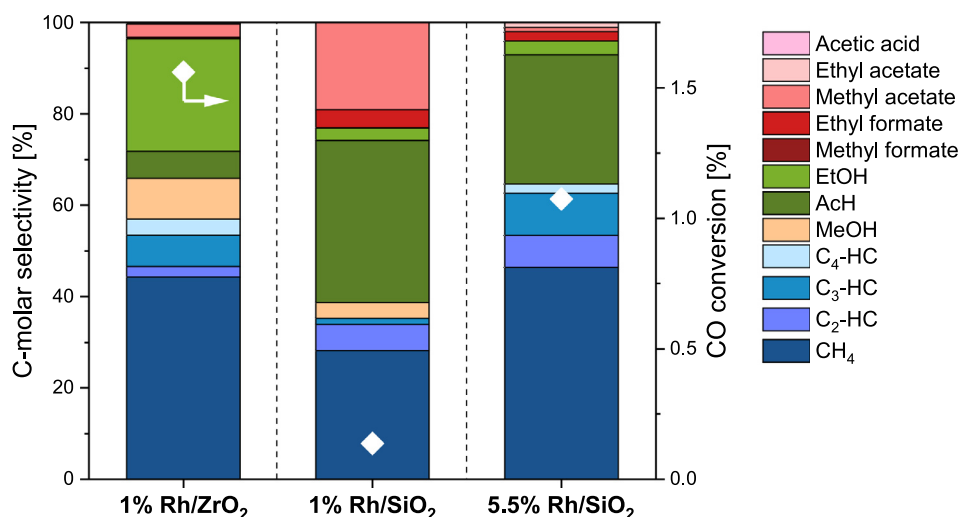

Fig. 2. Conversions and selectivities in CO hydrogenation with different supported Rh catalysts: 1 % Rh/ZrO$_2$, 1 % Rh/SiO$_2$ and 5.5 % Rh/SiO$_2$. Reaction conditions: 20 bar of CO/H$_2$ (V/V = 1/2), T = 250 °C for Rh/SiO$_2$ and 225 °C for 1 % Rh/ZrO$_2$, flow rate: 40 NmL min^{-1}, F/W = 4000 NmL min^{-1} g$_{Rh}^{-1}$.
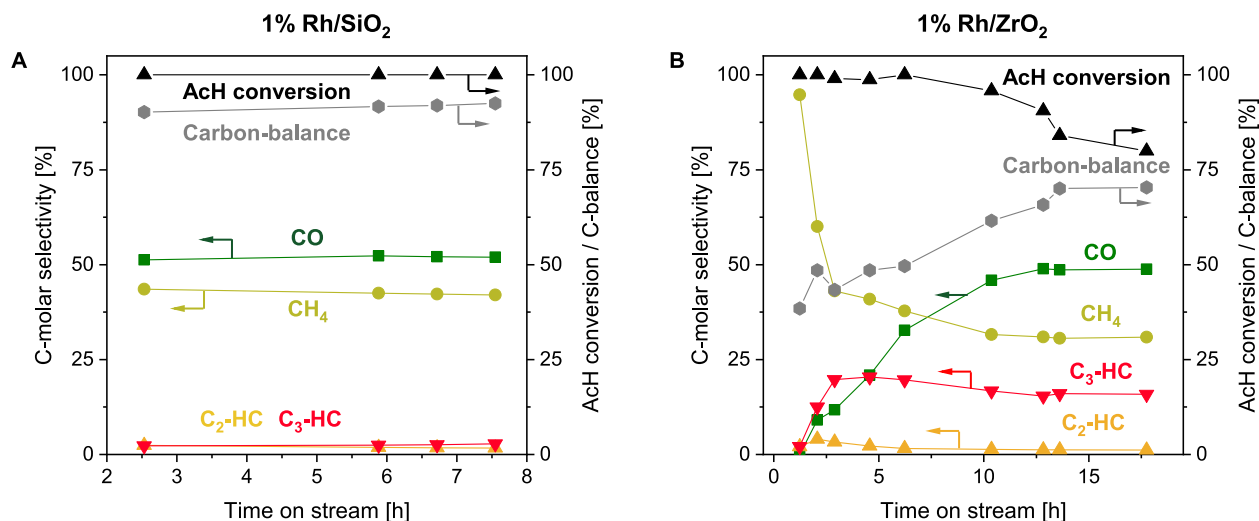
Fig. 3. The selectivity towards formed products (left Y-axis) and the AcH conversion level and the carbon balance (right Y-axis) when directing a reactant feed of 1598 ppm AcH in N_2 over 1 % Rh/SiO$_2$ (**A**) or 1 % Rh/ZrO$_2$ (**B**). Reaction conditions: 20 bar, T = 250 °C for 1 % Rh/SiO$_2$ and 225 °C for 1 % Rh/ZrO$_2$, catalyst mass = 1.00 g, flow rate = 40 NmL min^{-1} (see Table 1).

escape the reactor. The declining activity for aldehyde decomposition as the Rh surface is becoming filled with CO suggests that a sufficiently high CO coverage on the metal surface can protect the oxygenates from decomposition. Another interesting aspect of the aldehyde conversion over Rh/ZrO$_2$ is that, while the CO selectivity (50 %) suggests that all converted aldehyde is decarbonylated, the hydrocarbon products are a mixture of CH$_4$ and C$_3$-hydrocarbons. This can be understood from part of the acetaldehyde undergoing aldol condensation (likely ZrO$_2$-catalyzed) to croton aldehyde (CH$_3$CH=CHCHO) [42], prior to decarbonylation [43], which yields CO and a C$_3$-hydrocarbon.

For 1 % Rh/SiO$_2$, the carbon balance closes reasonably well (ca. 90 %) within the uncertainty that is to be expected when considering possible formation of stable carbonaceous species. In the case of 1 % Rh/ZrO$_2$ the carbon balance is more open - particularly during the initial period. A control experiment monitoring the effluent products when directing a flow of AcH/N$_2$ over metal-free m-ZrO$_2$ led to a comparable delay for the detection of acetaldehyde, which is therefore attributed to the uptake of AcH on the zirconia surface (see Fig. S2). This uptake of AcH on the support and the indicated tautomerization of acetaldehyde (crotonaldehyde was not followed by the gas product analysis) may be part of the reason for the poor mass balance in Fig. 3B.

The conversion of AcH was also investigated when co-feeding AcH with H$_2$ or with CO/H$_2$ over the 1 % Rh/SiO$_2$ and 1 % Rh/ZrO$_2$ samples. Fig. 4 shows an overview of the different compounds that were detected when directing AcH over the catalyst bed in the different reaction atmospheres. In an AcH/N$_2$ atmosphere a near complete decarbonylation of AcH occurs and yields an equimolar mixture of CO and hydrocarbons (Fig. 4A). When feeding acetaldehyde together with hydrogen (Fig. 4B) there is also full conversion, and CH$_4$ becomes the near-exclusive product, indicating a rapid methanation of CO formed via the decarbonylation of acetaldehyde. These results corroborate observations found in Rh single crystal studies [19,41] where oxygenates such as acetaldehyde were readily decomposed over the bare Rh surface. Fig. 4C shows the selectivity in AcH conversion, when AcH was co-fed with the CO/H$_2$ reaction feed (see also Tables S3-S6). This result is obtained by subtracting the productivity levels obtained in CO/H$_2$ from those in AcH/CO/H$_2$. Thus, a selectivity to acetaldehyde signifies that a fraction of the fed acetaldehyde passes unconverted through the reactor. Although a minor decomposition of the aldehyde also

occurs in the presence of CO, Fig. 4C clearly indicates that the predominant fraction of oxygenates is preserved. When compared to the complete AcH decomposition in the absence of CO (Fig. 4A and 4B) these results illustrate that a highly CO-covered metal surface is required to enable the preservation of oxygenate products. When co-fed with CO/H$_2$ acetaldehyde primarily passes through the reactor without being converted in the case of Rh/SiO$_2$ or is hydrogenated to ethanol in the case of Rh/ZrO$_2$. This illustrates that under high CO coverage conditions Rh/ZrO$_2$ maintains a hydrogenation activity that far exceeds the one of Rh/SiO$_2$. The preference for ethanol over acetaldehyde for Rh/ZrO$_2$ in steady state CO hydrogenation (Fig. 2) can thus be ascribed to an increased ability to hydrogenate formed acetaldehyde into ethanol rather than to the existence of a parallel pathway leading to ethanol.

The reason for the superior hydrogenation activity caused by the support effect from ZrO$_2$ cannot be fully identified on the basis of the presently available information. An indirect electronic effect of the adsorbates on the metal cannot be ruled out. The hydrogenation of acetaldehyde by hydrogen diffusing from the oxide support to the metal surface (i.e. spillover) can also not be ruled out in this case. The sticking coefficient of H$_2$ on Rh is normally orders of magnitude higher than on an oxide [44–46], and consequently the support would normally have a neglible contribution to hydrogen activation for Rh-containing catalysts. However, during CO hydrogenation the CO coverage on Rh may be so high that it limits the hydrogen activation on the metal to an extent that could make spillover of activated hydrogen from the support important.

While the results presented in Fig. 4 clearly show that a high CO coverage can prevent the otherwise readily occurring decomposition of C$_2$-oxygenates, they also underline that even over a highly CO-covered metal surface some decomposition occurs. Part of the oxygenates formed during CO hydrogenation reaction must thus be expected to decompose before escaping from the reactor. Consequently, the oxygenate selectivity levels that are determined from the reactor effluent, such as those in Fig. 2, are most likely lower than the selectivity in the primary reaction forming the oxygenates from CO and H$_2$.

3.4. Involvement of surface species on the support

It is well-established [23,47,48] that support/promotor materials leading to increased activity (such as ZrO$_2$) also result in an
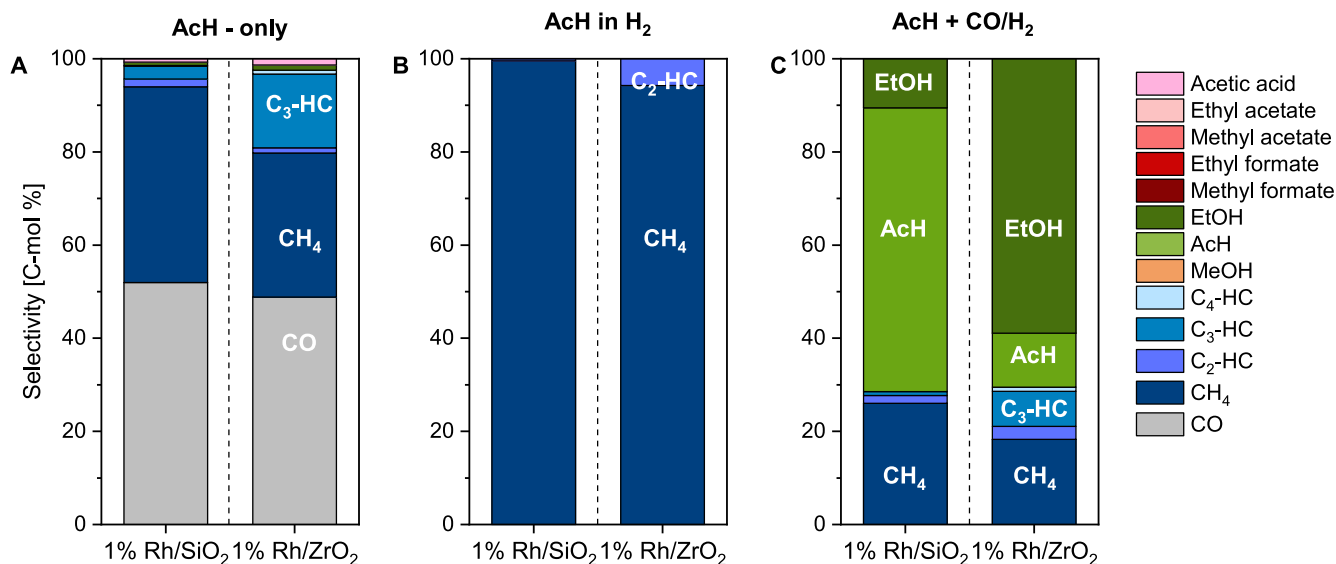
Fig. 4. The product distribution obtained from catalytic reaction tests studying the stability of AcH in different atmospheres over 1 wt% Rh supported on SiO_2 or ZrO_2. **A**: Selectivity in conversion of 1598 ppm AcH in N_2 (full AcH conversion is observed). **B**: Selectivity in conversion of 533 ppm AcH in 67 vol% H_2/33 vol%N_2 (full AcH conversion is observed). **C**: The net selectivities in conversion of 399 ppm AcH in a $CO/H_2/N_2$ (1/2/1) atmosphere. The results are corrected for the production from CO/H_2 alone under the same condition. Full reaction conditions are provided in Table 1.

increased presence of adsorbates on the support/promoter such as formates, acetates and alkoxides. The promotional effect could therefore arise from the emergence of bifunctional pathways via such species. If these species on the oxide are important reaction intermediates, they must be expected to react and disappear, if CO is removed from the feed. Fig. 5 shows DRIFTS spectra obtained from transient response experiments for Rh/ZrO_2. Here the catalyst was allowed to reach steady state during reaction in H_2/CO, whereupon the feeding of the CO reactant was stopped, while the hydrogen flow was maintained (retaining temperature and pressure).
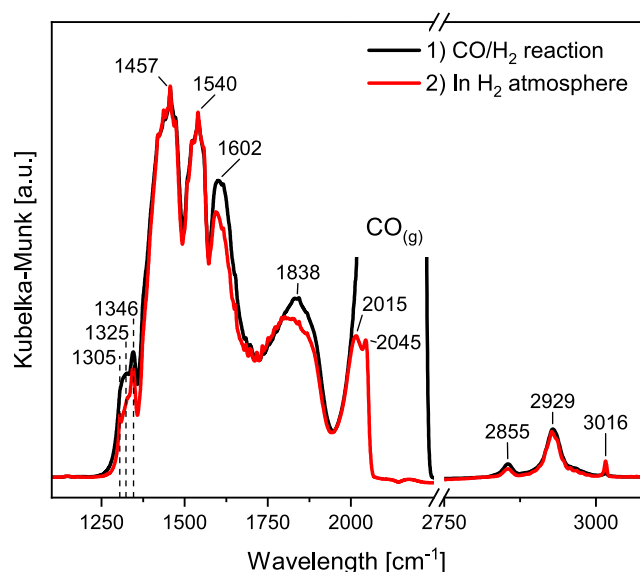

Fig. 5. DRIFTS spectra from transient response experiments over 1 % Rh/ZrO_2. Black line: spectrum recorded during catalytic reaction in a CO/H_2 atmosphere (16 bar of CO/H_2 (V/V = 1/2), T = 250 °C). Red line: spectrum after subsequent fading out of CO and running with pure H_2 at 13 bar and 250 °C for several hours. In addition to the assignments in the text the band at 1838 cm^{-1} is attributed to bridging bound CO on Rh [53] and the bands at 2015 and 2045 cm^{-1} are attributed to linear Rh-CO species. (For interpretation of the references to colour in this figure legend, the reader is referred to the web version of this article.)

Spectra recorded in the CO/H_2 atmosphere (black line) illustrate a substantial population of the Rh/ZrO_2 catalyst sample with different adsorbates. Intense absorption bands around 1460 and 1600 cm^{-1} indicate the presence of bicarbonate (HCO_3) species [49,50] on ZrO_2, and bands at 1346 and 1540 cm^{-1} indicate acetate (CH_3COO) species on ZrO_2 [51]. The presence of such adsorbates suggests a basic character of the ZrO_2 support. Weaker but distinct bands at 2855 and 2929 cm^{-1} also suggest the presence of methoxide (CH_3O) species [49,50,52] on ZrO_2. The presence of gaseous CH_4 was observed by an absorption band at 3016 cm^{-1}. The spectrum recorded several hours after switching from CO/H_2 to a pure H_2 atmosphere (red line) is nearly unaltered. This indicates a high stability of the adsorbate species that form on the support during the CO/H_2 reaction and strongly suggests the predominant fraction of these adsorbates to be spectator species. Species such as methoxide and acetate most likely form when C_1- and C_2-oxygenates created on the metal subsequently readsorb on the oxide. Because of their high stability these species on the oxide remain as spectators during the reaction. Similar observations were made for Rh/SiO_2, where methoxide on SiO_2 was the primary adsorbate on the support in CO/H_2 (see Fig. S3). Only slight decreases in the IR absorption band intensities for methoxide on SiO_2 were observed after switching to pure H_2 suggesting that the species on the support also possess a spectator role for Rh/SiO_2. From these results there is no indication that a bifunctional mechanism via adsorbate species associated with the support plays a major role for the support effect.

3.5. Temperature programmed hydrogenation experiments

To obtain further insight into the reaction mechanism and its dependence on the support, the catalysts were subjected to temperature programmed hydrogenation experiments. Catalysts were allowed to reach steady state in CO/H_2 at 16 bar and 250 °C reaction, and then rapidly (~3 min) cooled down to 30 °C in the reaction atmosphere to preserve the species on the surface. After residual gaseous CO was purged by He the samples were subjected to temperature programmed hydrogenation (TPH) in flowing H_2 at atmospheric pressure, while the surface species were monitored by DRIFTS (see Fig. S4-S6) and the reactor effluent was monitored by

MS analysis. Fig. 6 shows the MS signal signals associated with methane (m/z = 15) and C_2-oxygenates (followed by the acetyl CH_3CO fragment, m/z = 43) along with the normalized IR signal intensity for the linearly bound Rh-CO species during the TPH for Rh/SiO$_2$ (Fig. 6A) and Rh/ZrO$_2$ (Fig. 6B). Under certain conditions Rh *gem*-dicarbonyls can form in CO containing atmospheres [54,55]. However, in the present work IR spectroscopy (Fig. S4 – S7, S9) only showed linearly bound CO on the surface of metallic Rh nanoparticles. Hence all conclusions in the present work must relate to surface species on metallic Rh nanoparticles.

Fig. 6A clearly shows that for Rh/SiO$_2$ the methane formation correlates well with the disappearance of adsorbed CO. As no other surface species could be observed to change in this temperature range this suggests that CO dissociation is the rate limiting step in the reaction, and that all intermediates between CO and CH$_4$ are too short-lived to be followed by IR spectroscopy at temperatures above ca. 200 ℃ where the CO activation occurs in Fig. 6A. A minor evolution of C_2-oxygenates also occurs in the early part of the conversion of the adsorbed CO. For the parallel experiment with Rh/ZrO$_2$ (Fig. 6B) the main observation is that elimination of the CO surface species is shifted down in temperature relative to Rh/SiO$_2$. Negligible molecular CO desorption was observed in the temperature region where the major decrease in IR signal intensity for Rh-CO is observed (Fig. 7). This shows that the elimination of CO primarily is by dissociation. That CO in disappears at a lower temperature on Rh/ZrO$_2$ (ca. 200 ℃) than on Rh/SiO$_2$ (ca. 250 ℃) in Fig. 6 therefore suggests that the rate limiting C-O dissociation on Rh is accelerated by the ZrO$_2$ support. This is in agreement with the faster steady state reaction over Rh/ZrO$_2$ (Fig. 1). For Rh/ZrO$_2$ the methane formation in the TPH experiment is larger and extends to far higher temperatures. This can be correlated to the gradual conversion of the high concentration of carbon-containing surface species present on the support during the reaction (see Fig. 5) and potentially also conversion of carbonaceous deposits on the surface. Since numerous species contribute to methane formation in the TPH for Rh/ZrO$_2$ it is difficult to fully delineate the methane formation arising from CO on the Rh surface.

Fig. 6 shows that catalysts exposed to reaction conditions do not yield significant CO dissociation during subsequent TPH until ca. 200 °C. Interestingly, previous work on promoted Rh/SiO$_2$ catalysts has shown that methane formation during TPH can occur below 200 °C and the major difference is that those studies preadsorbed CO at ambient temperature [56,57]. To gain further insight into the CO dissociation we compared the TPH after exposure to reaction conditions in Fig. 6 to a TPH after CO-preadsorption at 30 °C. Fig. 7A shows a comparison of the CH$_4$ formation and the relative CO coverage during TPH after exposure to reaction conditions (CO/H$_2$ at 16 bar and 250 °C) or exposure to 9.5 vol% CO at 30 °C and atmospheric pressure. Fig. 7B shows the evolution of gaseous, molecular CO during the two TPH experiments. Fig. 7A illustrates that after low-temperature CO adsorption, the CO activation, evidenced by methane formation, sets in at around 75 °C, whereas after the high-temperature adsorption CO activation only sets in at ca. 200 °C. This can be rationalized by the CO desorption in Fig. 7B, which illustrates that in both cases an initial desorption of molecular CO has to take place. The completion of this initial desorption occurs at 75 °C after low-temperature adsorption and at 200 °C after high temperature adsorption, which correlates very well to the emergence of CO activation/methane formation in the two cases. In both cases, the Rh surface thus adsorbs so much CO, that it is prohibitive to the CO activation, and part of the CO has to desorb before any CO hydrogenation can occur. After high-temperature adsorption, this initial desorption is not completed until higher temperatures, which suggests an increased stability of the adsorbed CO. The adsorption of CO from synthesis gas at the higher temperatures is therefore concluded to lead to a rearrangement in the adsorbate layer that results in a stronger bonding of the adsorbed CO. As a result of the stabilization of the CO adlayer at higher temperature, the onset of CO activation in the subsequent TPH thus becomes dependent on the adsorption conditions. Since the integral amount of CO that has to desorb before CO activation can take place is also greater after high-temperature adsorption, the coverage with inhibiting CO must also be increased by this rearrangement. The results thus indicate an activated rearrangement in the adsorbate layer that increases both the stability and possibly also the coverage of adsorbed CO. Whether this rearrangement only involves the adlayer or also the underlying metal surface cannot be determined from the present data. This activated adsorption of CO does not appear to be limited to Rh. Loveless *et al.* [58] observed an increased CO uptake with increasing
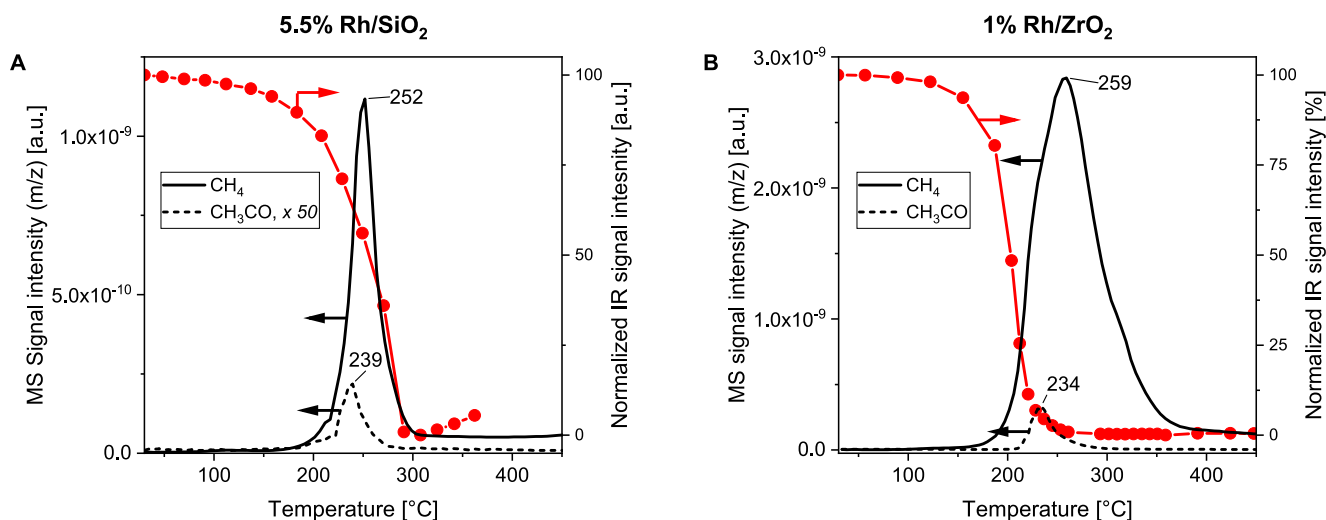

Fig. 6. Comparison of the the MS signals assigned to CH$_4$ (m/z = 15, black line) and C_2-oxygenates (CH$_3$O fragment, m/z = 43, black dashed line) and the normalized signal intensity of infrared absorption bands for Rh-CO$_{lin}$ species (right Y–axis, red line) that were obtained during TPH sequences for 5.5 % Rh/SiO$_2$ (**A**) and 1 % Rh/ZrO$_2$ (**B**). Prior to the TPH sequence in H$_2$ (ramp rate: 5 °C/min, 1 bar, 40 mL min^{-1}), the catalysts were treated to CO/H$_2$ reaction conditions (16 bar of CO/H$_2$/Ar (V/V/V = 1/2/9), T = 250 °C, flow rate = 40 mL min^{-1}) for 2 h. The amounts of Rh surface sites present in the experiments are 6 µmol for Rh/SiO$_2$ and 4 µmol for Rh/ZrO$_2$. (For interpretation of the references to colour in this figure legend, the reader is referred to the web version of this article.)
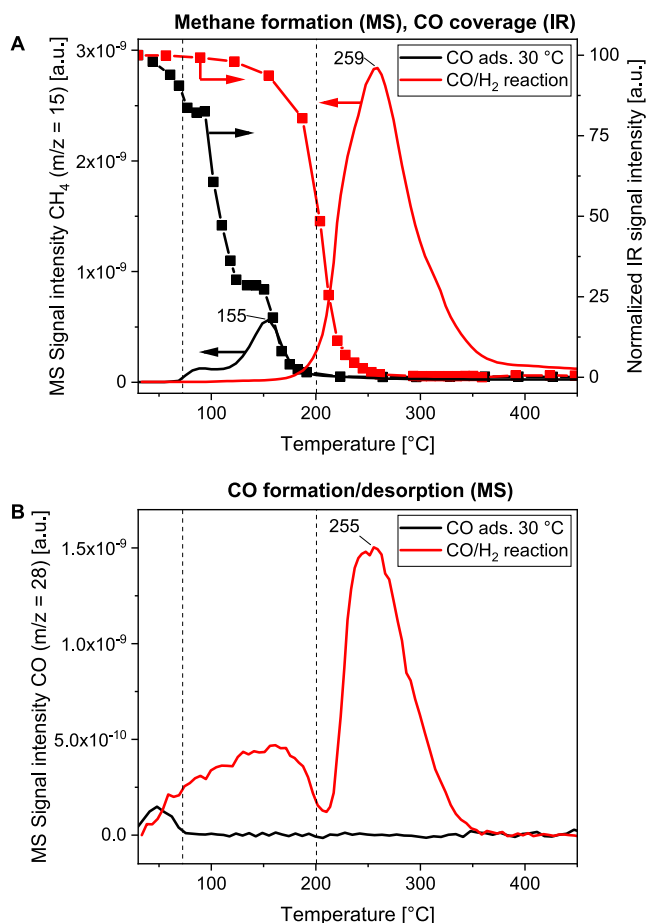
Fig. 7. TPH experiments for 1 % Rh/ZrO$_2$ after CO pre-adsorption at 30 °C or after CO/H$_2$ at 250 °C. **A** Methane formation (m/z = 15) and normalized IR absorption band intensity for Rh-CO$_{lin}$ species (2067 cm^{-1}) as functions of temperature during TPH. **B** The evolution of gaseous CO (m/z = 28) during TPH. Dashed lines illustrate the correlation between completion of the initial CO desorption and the onset of CO activation evident from methane formation. The low temperature CO desorption (<200 °C) is attributed to molecular desorption of pre-adsorbed CO, whereas the major CO desorption peak at 200–350 °C is attributed to recombination of already dissociated C and O since this desorption occurs after disappearance of the CO IR signals. Different pretreatments were applied before TPH. Black line: 30 min exposure to 9.5 % CO/Ar at 30 °C, red line: catalytic reaction treatment in 16 bar of CO/H$_2$/Ar (V/V/V = 1/2/9) at 250 °C before being quenched in reaction atmosphere. (For interpretation of the references to colour in this figure legend, the reader is referred to the web version of this article.)

temperature for Ru/SiO$_2$, but did not investigate the stability of the adsorbed CO. Similarly, Falconer and co-workers inferred an increased CO coverage from TPH results after high-temperature CO adsorption for Ru/Al$_2$O$_3$ [59], Ni/Al$_2$O$_3$ [60,61] and Ni/TiO$_2$ [62]. That part of the CO coverage has to desorb before CO activation becomes possible was also observed for silica supported Rh (see Figure S8), so this prohibitively high coverage is not support dependent. The phenomenon is also not specific to Rh, as the same behavior is evident in previous studies of Ni/Al$_2$O$_3$ [61] and Pd-based catalysts [63]. However, the correlation between the desorption of this blocking CO and the onset of an ability to activate CO does not appear to have been identified previously, but is clear from the results in Fig. 7. Given the generality of this activated CO adsorption behavior, and the necessity for desorption of prohibitive CO, prior to CO activation, the conclusions made here for Rh are very likely to be relevant for CO hydrogenation over other metals as well.

Because CO desorption and hydrogenation occur at a lower temperature after CO pre-adsorption at 30 °C, it is possible to observe surface species that are too short-lived to be monitored during steady state reaction at higher temperatures. Here, this allows the detection of a hydrogen-assisted pathway of CO activation. Fig. 8A shows the methane formation and the development in selected IR signals during TPH after CO adsorption on Rh/ZrO$_2$ at 30 °C. The results illustrate that the initial CO conversion at 75 – 120 °C leads to a species characterized by two IR bands at 2821 cm^{-1} and 2927 cm^{-1}. These bands correspond well to C-H stretches in methoxide species on a metal surface [64–69] and are clearly different from the bands arising from methoxide species on the ZrO$_2$ surface (as shown in Fig. 8B). At 120 – 175 °C the methoxide on the metal is then converted into methane as evident from the correlated disappearance of methoxide IR signals and appearance of a methane MS signal. These results provide clear evidence for the existence of a H-assisted CO dissociation pathway via CH$_3$O on the Rh surface. This is in good agreement with DFT calculations on Rh(111) by Choi and Liu [17], which identified a H-assisted pathway via methoxide with surmountable barriers. Moreover, the observation of C-O scission via CH$_3$O is in good agreement with the detection of methoxide species on Rh(111) and Rh(211) single crystal surfaces in a CO/H$_2$ atmosphere during operando ambient pressure X-ray photoelectron spectroscopy experiments [70]. This observation of a hydrogen-assisted CO activation via methoxide also reconciles why the CO conversion on Rh exhibits an inverse H/D isotope effect [15,16] despite the C-O dissociation being rate limiting. Furthermore, the observation of a mechanism via a rate limiting C-O bond breakage in methoxide can explain the nature of the isotope effects. In adsorbed methoxide the stronger bonds to the heavier deuterium lead to a weaker C-O bond (evident from a lower C-O stretching frequency [64]) in CD$_3$O compared to CH$_3$O, and this weakening of the C-O bond is the reason for the higher reaction rate from D$_2$ compared to H$_2$.

The observation of the methoxide pathway after low temperature CO pre-adsorption raises the question of whether this pathway is also relevant for the steady state reaction at higher temperatures. For the Rh/ZrO$_2$ catalyst subjected to steady state reaction in CO/H$_2$ (Fig. 8B) or to subsequent TPH (spectra shown in Fig. S9) there are strong bands at 2851 cm^{-1} and 2921 cm^{-1} attributable to species on the ZrO$_2$ support which prevent detailed monitoring of the methoxide species on the metal. Additionally, the results in Fig. 8A suggest that conversion of methoxide on the metal is rapid above 175 °C, which should lead to a small population of such species at higher temperatures. However, methoxide on Rh could be observed transiently, when changing from a CO feed to pure H$_2$ under reaction temperature and pressure conditions (see Fig. S10). Combined with the fact that the hydrogen assisted pathway can explain the inverse H/D isotope effect observed [15,16] for both Rh/ZrO$_2$ and Rh/SiO$_2$ this would suggest that the methoxide pathway is important for the steady state CO hydrogenation over Rh catalysts.

Since the rate-limiting CO activation appears to be hydrogen assisted (via CH$_3$O), there is a consistency between the higher rates with Rh/ZrO$_2$ and the shift in oxygenate distribution towards ethanol for this catalyst. Both observations suggest that at least part of the support effect from ZrO$_2$ is that it enables a higher hydrogenation activity of the Rh surface during reaction conditions. However, DRIFTS spectra recorded for the supported Rh catalysts after exposure to CO at elevated temperature and pressure conditions also reveal a redshift in the C-O stretch for CO adsorbed on Rh/ZrO$_2$ (2029 cm^{-1}) compared to Rh/SiO$_2$ (2043 – 2062 cm^{-1}) (Fig. S11). So, it is possible that a support induced weakening of the C-O bond in CO adsorbed on Rh/ZrO$_2$ also plays a role in the support effect. This is consistent with the greater tendency for Rh/ZrO$_2$ to adsorb the CO formed during acetaldehyde decarbonylation (Fig. 3), which also suggests that ZrO$_2$ induces a stronger interaction between Rh and CO that weakens the internal C-O bond in the adsorbed CO.
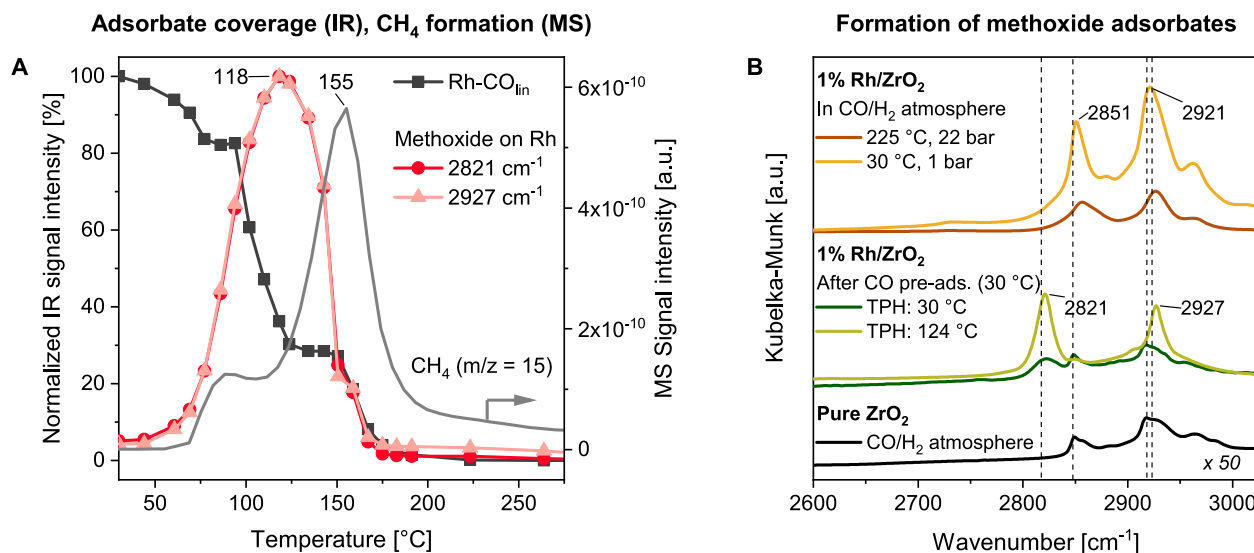
Fig. 8. A Normalized IR signal intensities (left Y-axis) assigned to Rh-CO$_{lin}$ (2067 cm^{-1}) and CH$_3$O-Rh species on the Rh metal (2821 and 2927 cm^{-1}), as well as the evolution of methane (right Y-axis) detected by MS (*m/z* = 15) as functions of temperature during a TPH sequence over 1 % Rh/ZrO$_2$. The reduced catalyst was, at atmospheric pressure, pre-covered with CO from a flow of 9.5 % CO/Ar at 30 °C and subsequently purged with He before TPH. **B** The upper two spectra refer to 1 % Rh/ZrO$_2$ after treatment in CO/H$_2$ (250 °C, 16 bar) and subsequent quenching in CO/H$_2$ (to 30 °C, 1 bar). The middle two spectra relate to 1 % Rh/ZrO$_2$ after being pre-adsorbed with 9.5 % CO/Ar at 30 °C, then purged with He and subsequently subjected to TPH. Spectra were recorded at different temperatures during the TPH. The lower spectrum refers to pure ZrO$_2$ after being first treated in CO/H$_2$ (250 °C, 18 bar) and subsequently quenched in CO/H$_2$ reaction atmosphere (to 30 °C, 1 bar).

4. Conclusions

The present study has investigated the mechanism, surface species and support effects in the Rh-catalyzed CO hydrogenation using catalysts with small Rh particles where oxygenates are a significant fraction of the reaction product. The reaction shows a strong support effect with Rh/ZrO$_2$ yielding a steady state CO conversion that is at least an order of magnitude higher than the one for Rh/SiO$_2$. TPH experiments after CO pre-adsorption strongly suggest that dissociation of CO on the metallic surface is the rate limiting step in the CO hydrogenation and that the ZrO$_2$ support enhances this dissociation step compared to Rh on SiO$_2$. Infrared measurements after stopping the CO-flow at steady state conditions suggest that the adsorbates associated with ZrO$_2$ are too stable to be reaction intermediates. Consequently, the support effect is not the result of a bifunctional mechanism involving species on or associated with the ZrO$_2$, but rather evolves as an impact of ZrO$_2$ on the dissociation of CO on the metallic surface. TPH after pre-adsorption of CO on Rh/ZrO$_2$ at ambient temperature reveals the existence of a hydrogen-assisted CO activation pathway that proceeds through methoxide species binding on the metal surface. Observation of such a H-containing CO species as the precursor for subsequent dissociative CO activation is also in line with previous theoretical and experimental studies. Furthermore, this hydrogen-assisted mechanism can explain why an H/D isotope effect has previously been observed for both Rh/ZrO$_2$ and Rh/SiO$_2$ despite the CO dissociation being the rate limiting step.

In the presence of CO/H$_2$ at higher temperatures characteristic of the CO hydrogenation reaction, there is an activated process which increases both the stability and the coverage of adsorbed CO. Both pre-adsorption of CO from a flow of dilute CO at 30 °C and from a CO/H$_2$ flow at 250 °C leads to a high CO uptake that is prohibitive to CO activation. In a subsequent TPH part of this inhibiting CO has to desorb before any CO activation can occur. The stabilizing re-arrangement of the CO adlayer occurring at higher temperature shifts this initial desorption towards higher temperature and thus delays the onset of CO activation in the TPH experiment. Certain properties observed here for Rh, such as

the shift towards increased CO coverage at higher temperature and the necessity for desorption of part of the CO prior to commencement of CO activation, can also be identified in the literature for other metals, such as Ru, Ni and Pd. Due to these similarities, the present conclusions concerning the activated stabilization of CO adlayer and the nature of the hydrogen-assisted CO activation via CH$_3$O could be of general significance for metal-catalyzed CO hydrogenation on other metals.

Another support effect in the Rh-catalyzed CO hydrogenation is that ethanol is the dominant oxygenate formed over Rh/ZrO$_2$ while acetaldehyde dominates over Rh/SiO$_2$. Experiments with acetaldehyde conversion in various atmospheres reveal that the ability of supported Rh catalysts to produce C_2-oxygenates at desirable selectivity levels is intrinsically linked to a highly CO-covered metal surface, which prevents the decomposition of oxygenates that is facile over a bare Rh metal surface. At the high CO coverage characteristic of the CO hydrogenation reaction, the fraction of oxygenates being decomposed by Rh is found to be relatively limited. However, on a highly CO covered surface Rh/ZrO$_2$ retains an ability to hydrogenate acetaladehyde, whereas the CO covered Rh surface of Rh/SiO$_2$ is largely unable to hydrogenate acetaldehyde. Considering the observation of hydrogen assisted CO activation via CH$_3$O, both the higher CO hydrogenation rates and the shift in oxygenates towards ethanol for Rh/ZrO$_2$ are consistent with part of the ZrO$_2$ support effect being an increased hydrogenation ability at the CO-covered state of the working catalyst.

Data availability

Data will be made available on request.

Declaration of Competing Interest

The authors declare that they have no known competing financial interests or personal relationships that could have appeared to influence the work reported in this paper.

Acknowledgements

Appendix A. Supplementary data

Supplementary data to this article can be found online at https://doi.org/10.1016/j.jcat.2022.08.031.

References

[1] J.J. Spivey, A. Egbebi, Heterogeneous catalytic synthesis of ethanol from biomass-derived syngas, Chem. Soc. Rev. 36 (2007) 1514, https://doi.org/10.1039/b414039g.

[2] H.T. Luk, C. Mondelli, D.C. Ferré, J.A. Stewart, J. Pérez-Ramírez, Status and prospects in higher alcohols synthesis from syngas, Chem. Soc. Rev. 46 (2017) 1358–1426, https://doi.org/10.1039/c6cs00324a.

[3] C.F. Shih, T. Zhang, J. Li, C. Bai, Powering the Future with Liquid Sunshine, Joule. 2 (2018) 1925–1949, https://doi.org/10.1016/j.joule.2018.08.016.

[4] V. Ponec, Chapter 4 Selectivity in The Syngas Reactions: The Role of Supports and Promoters in The Activation of CO and In The Stabilization of Intermediates, Stud. Surf. Sci. Catal. 64 (1991) 117–157, https://doi.org/10.1016/S0167-2991(08)60946-5.

[5] W.M.H. Sachtler, D.F. Shriver, M. Ichikawa, The formation of C_2-oxygenates from synthesis gas over oxide-supported rhodium. Reply to van der Lee and Ponec, J. Catal. 99 (1986) 513–514, https://doi.org/10.1016/0021-9517(86)90378-7.

[6] M. Ichikawa, Catalysis by Supported Metal Crystallites from Carbonyl Clusters. II. Catalytic Ethanol Synthesis from CO and H_2 under Atmospheric Pressure over Supported Rhodium Crystallites Prepared from Rh Carbonyl Clusters Deposited on TiO_2, ZrO_2, and La_2O_3, Bull. Chem. Soc. Jpn. 51 (1978) 2273–2277, https://doi.org/10.1246/bcsj.51.2273.

[7] R.P. Underwood, A.T. Bell, CO hydrogenation over rhodium supported on SiO_2, La_2O_3, Nd_2O_3 and Sm_2O_3, Appl. Catal. 21 (1986) 157–168, https://doi.org/10.1016/S0166-9834(00)81336-6.

[8] J. Yu, D. Mao, L. Han, Q. Guo, G. Lu, The effect of Fe on the catalytic performance of Rh-Mn-Li/SiO_2 catalyst: A DRIFTS study, Catal. Commun. 27 (2012) 1–4, https://doi.org/10.1016/j.catcom.2012.06.010.

[9] Z. Guo, J. Liu, J.T. Miller, R. Tao, R.J. Meyer, J.R. Regalbuto, C.L. Marshall, R.F. Klie, Selective Adsorption of Manganese onto Rhodium for Optimized Mn/Rh/SiO_2 Alcohol Synthesis Catalysts, ChemCatChem. 5 (2013) 3665–3672, https://doi.org/10.1002/cctc.201300479.

[10] M. Ichikawa, T. Fukushima, Mechanism of Syngas Conversion into C_2-oxygenates such as Ethanol catalysed on a SiO_2-supported Rh–Ti Catalyst, J. Chem. Soc., Chem. Commun. 101 (1985) 321–323, https://doi.org/10.1039/C39850000321.

[11] I.A.W. Filot, R.J.P. Broos, J.P.M. Van Rijn, G.J.H.A. Van Heugten, R.A. Van Santen, E.J.M. Hensen, First-Principles-Based Microkinetics Simulations of Synthesis Gas Conversion on a Stepped Rhodium Surface, ACS Catal. 5 (2015) 5453–5467, https://doi.org/10.1021/acscatal.5b01391.

[12] N. Yang, A.J. Medford, X. Liu, F. Studt, T. Bligaard, S.F. Bent, J.K. Nørskov, Intrinsic Selectivity and Structure Sensitivity of Rhodium Catalysts for C_{2+} Oxygenate Production, J. Am. Chem. Soc. 138 (2016) 3705–3714, https://doi.org/10.1021/jacs.5b12087.

[13] H.T. Luk, C. Mondelli, D.C. Ferré, J.A. Stewart, J. Pérez-Ramírez, Chem Soc Rev Status and prospects in higher alcohols synthesis from syngas, Chem. Soc. Rev. 46 (5) (2017) 1358–1426, https://doi.org/10.1039/C6CS00324A.

[14] M. Dimitrakopoulou, X. Huang, J. Kröhnert, D. Teschner, S. Praetz, C. Schlesiger, W. Malzer, C. Janke, E. Schwab, F. Rosowski, H. Kaiser, S. Schunk, R. Schlögl, A. Trunschke, Insights into structure and dynamics of (Mn, Fe)O_x-promoted Rh nanoparticles, Faraday Discuss. 208 (2018) 207–225, https://doi.org/10.1039/c7fd00215g.

[15] T. Iizuka, Y. Tanaka, K. Tanabe, Hydrogenation of CO and CO_2 over rhodium catalysts supported on various metal oxides, J. Catal. 76 (1982) 1–8, https://doi.org/10.1016/0021-9517(82)90230-5.

[16] H. Wang, J. Liu, J. Fu, H. Wan, K. Tsai, Study on the mechanism of ethanol synthesis from syngas by in-situ chemical trapping and isotopic exchange reactions, Catal. Letters. 12 (1992) 87–96, https://doi.org/10.1007/BF00767191.

[17] Y. Choi, P. Liu, Mechanism of Ethanol Synthesis from Syngas on Rh(111), J. Am. Chem. Soc. 131 (2009) 13054–13061, https://doi.org/10.1021/ja903013x.

[18] N. Yang, J.S. Yoo, J. Schumann, P. Bothra, J.A. Singh, E. Valle, F. Abild-pedersen, J. K. Nørskov, S.F. Bent, Rh-MnO Interface Sites Formed by Atomic Layer Deposition Promote Syngas Conversion to Higher Oxygenates, ACS Catal. 7 (2017) 5746–5757, https://doi.org/10.1021/acscatal.7b01851.

[19] C.J. Houtman, M.A. Barteau, Divergent pathways of acetaldehyde and ethanol decarbonylation on the Rh(111) surface, J. Catal. 130 (1991) 528–546, https://doi.org/10.1016/0021-9517(91)90133-O.

[20] C.J. Houtman, N.F. Brown, M.A. Barteau, The Chemistry of Acetates on the Rh (111) Surface, J. Catal. 145 (1994) 37–53, https://doi.org/10.1006/jcat.1994.1005.

[21] N.F. Brown, M.A. Barteau, Activation of C-H, C-C, and C-O Bonds of Oxygenates on Rh(111), ACS Symp. Ser. 517 (1993) 345–354, https://doi.org/10.1021/bk-1993-0517.ch024.

[22] D. Demri, J. Hindermann, C. Diagne, A. Kiennemann, Formation of C_2-Oxygenates on Rhodium-containing Catalysts during CO + H_2 Reactions, J. Chem. Soc. Faraday Trans. 90 (1994) 501–506, https://doi.org/10.1039/FT9949000501.

[23] J.C. Lavalley, J. Saussey, J. Lamotte, R. Breault, J.P. Hindermann, A. Kiennemann, Infrared study of carbon monoxide hydrogenation over rhodium/ceria and rhodium/silica catalysts, J. Phys. Chem. 94 (1990) 5941–5947, https://doi.org/10.1021/j100378a061.

[24] J. Zhang, X.M. Cao, P. Hu, Z. Zhong, A. Borgna, P. Wu, Density functional theory studies of ethanol decomposition on Rh(211), J. Phys. Chem. C. 115 (2011) 22429–22437, https://doi.org/10.1021/jp206837z.

[25] Y. Choi, P. Liu, Understanding of ethanol decomposition on Rh(111) from density functional theory and kinetic Monte Carlo simulations, Catal. Today. 165 (2011) 64–70, https://doi.org/10.1016/j.cattod.2010.12.017.

[26] M. Kawai, M. Uda, M. Ichikawa, The electronic state of supported rhodium catalysts and the selectivity for the hydrogenation of carbon monoxide, J. Phys. Chem. 89 (1985) 1654–1656, https://doi.org/10.1021/j100255a020.

[27] A. Boffa, C. Lin, A.T. Bell, G.A. Somorjai, Promotion of CO and CO_2 Hydrogenation over Rh by Metal Oxides: The Influence of Oxide Lewis Acidity and Reducibility, J. Catal. 149 (1994) 149–158, https://doi.org/10.1006/jcat.1994.1280.

[28] A. Takeuchi, J.R. Katzer, Ethanol Formation Mechanism from CO + H_2, J. Phys. Chem. 86 (1982) 2438–2441, https://doi.org/10.1021/j100210a038.

[29] H. Orita, S. Naito, K. Tamaru, Mechanism of Formation of C_2-Oxygenated Compounds from CO + H_2 Reaction over SiO_2-Supported Rh Catalysts, J. Catal. 90 (1984) 183–193, https://doi.org/10.1016/0021-9517(84)90247-1.

[30] A. Deluzarche, J.P. Hindermann, R. Kieffer, R. Breault, A. Kiennemann, Ethanol Formation Mechanism from CO + H_2 on a Rh/TiO_2 Catalyst, J. Phys. Chem. 88 (1984) 4993–4995, https://doi.org/10.1021/j150665a040.

[31] M. Ichikawa, Surface-Supported Metal Clusters and their Catalysis in CO-Based Reactions, in: Y. Iwasawa (Ed.), Tailored Met. Catal., D. Reidel Publishing Company, 1986, https://doi.org/10.1007/978-94-009-5261-4_4.

[32] A.L. Borer, C. Bronnimann, R. Prins, ZrO_2-Promoted Rh/SiO_2 Catalysts in CO Hydrogenation and Temperature-Programmed Reduction, J. Catal. 145 (2) (1994) 516–525, https://doi.org/10.1006/jcat.1994.1062.

[33] L. Han, D. Mao, J. Yu, Q. Guo, G. Lu, C_2-oxygenates synthesis through CO hydrogenation on SiO_2-ZrO_2 supported Rh-based catalyst: The effect of support, Appl. Catal. A Gen. 454 (2013) 81–87, https://doi.org/10.1016/j.apcata.2013.01.008.

[34] J.M. Christensen, P.M. Mortensen, R. Trane, P.A. Jensen, A.D. Jensen, Effects of H_2S and process conditions in the synthesis of mixed alcohols from syngas over alkali promoted cobalt-molybdenum sulfide, Appl. Catal. A Gen. 366 (2009) 29–43, https://doi.org/10.1016/j.apcata.2009.06.034.

[35] N.D. Nielsen, J. Thrane, A.D. Jensen, J.M. Christensen, Bifunctional Synergy in CO Hydrogenation to Methanol with Supported Cu, Catal. Letters. 150 (2020) 1427–1433, https://doi.org/10.1007/s10562-019-03036-7.

[36] H. Arakawa, K. Takeuchi, T. Matsuzaki, Y. Sugi, Effect of metal dispersion on the acitivty and selectivity of Rh/SiO_2 catalyst for high pressure CO hydrogenation, Chem. Lett. 1607–1610 (1984), https://doi.org/10.1246/cl.1984.1607.

[37] M. Schumann, M.R. Nielsen, T.E.L. Smitshuysen, T.W. Hansen, C.D. Damsgaard, A.-C.-A. Yang, M. Cargnello, J.-D. Grunwaldt, A.D. Jensen, J.M. Christensen, Rationalizing an Unexpected Structure Sensitivity in Heterogeneous Catalysis - CO Hydrogenation over Rh as a Case Study, ACS Catal. 11 (2021) 5189–5201, https://doi.org/10.1021/acscatal.0c05002.

[38] D.A.J.M. Ligthart, I.A.W. Filot, A.A.H. Almutairi, E.J.M. Hensen, Identification of step-edge sites on Rh nanoparticles for facile CO dissociation, Catal. Commun. 77 (2016) 5–8, https://doi.org/10.1016/j.catcom.2016.01.006.

[39] B.J. Kip, F.B.M. Duivenvoorden, D.C. Koningsberger, R. Prins, Determination of Metal Particle Size of Highly Dispersed Rh, Ir, and Pt Catalysts by Hydrogen Chemisorption and EXAFS, J. Am. Chem. Soc. 108 (1986) 5633–5634, https://doi.org/10.1021/ja00278a049.

[40] F. Drault, C. Comminges, F. Can, L. Pirault-Roy, F. Epron, A. Le Valant, Palladium, Iridium, and Rhodium Supported Catalysts: Predictive H_2 Chemisorption by Statistical Cuboctahedron Clusters Model, Materials (Basel). 11 (5) (2018) 819, https://doi.org/10.3390/ma11050819.

[41] E. Vesselli, A. Baraldi, G. Comelli, S. Lizzit, R. Rosei, Ethanol decomposition: C-C cleavage selectivity on Rh(111), ChemPhysChem. 5 (2004) 1133–1140, https://doi.org/10.1002/cphc.200400043.

[42] V.L. Sushkevich, I.I. Ivanova, Mechanistic study of ethanol conversion into butadiene over silver promoted zirconia catalysts, Appl. Catal. B Environ. 215 (2017) 36–49, https://doi.org/10.1016/j.apcatb.2017.05.060.

[43] H. Bock, O. Breuer, Decarbonylation on Carbon-Supported Nickel Catalysts, Angew. Chemie - Int. Ed. 26 (5) (1987) 461–462, https://doi.org/10.1002/anie.198704611.

[44] M. Ehsasi, K. Christmann, The interaction of hydrogen with a rhodium (110) surface, Surf. Sci. 194 (1988) 172–198, https://doi.org/10.1016/0039-6028(94)91253-X.

[45] M. Kunat, U. Burghaus, C. Wöll, Adsorption of hydrogen on the polar O-ZnO surface: A molecular beam study, Phys. Chem. Chem. Phys. 5 (2003) 4962–4967, https://doi.org/10.1039/b307955d.

[46] W. Nichtl-Pecher, W. Stammler, K. Heinz, K. Müller, Hydrogen on rhodium (311): Commensurate adsorption phases, reconstruction, and subsurface binding states, Phys. Rev. B. 43 (1991) 6946–6951, https://doi.org/10.1103/PhysRevB.43.6946.

[47] T. Fukushima, H. Arakawa, M. Ichikawa, In Situ High-pressure FT-IR Studies on the Surface Species Formed in CO Hydrogenation on SiO_2-Supported Rh-Fe Catalysts, J. Phys. Chem. 89 (1985) 4440–4443, https://doi.org/10.1021/j100267a009.

[48] T. Fukushima, H. Arakawa, M. Ichikawa, Spectroscopic Evidence of Acetyl and Acetate Species Directly Formed in $CO-H_2$ Conversion on SiO_2-Supported Rh and Rh-Mn Catalysts, J. Chem. Soc. Chem. Commun. (11) (1985) 729–731, https://doi.org/10.1039/c39850000729.

[49] E. Guglielminotti, Infrared Study of Syngas Adsorption on Zirconia, Langmuir. 6 (1990) 1455–1460, https://doi.org/10.1021/la00099a005.

[50] M.Y. He, J.G. Ekerdt, Infrared studies of the adsorption of synthesis gas on zirconium dioxide, J. Catal. 87 (1984) 381–388, https://doi.org/10.1016/0021-9517(84)90198-2.

[51] K.D. Dobson, A.J. McQuillan, In situ infrared spectroscopic analysis of the adsorption of aliphatic carboxylic acids to TiO_2, ZrO_2, Al_2O_3, and Ta_2O_5 from aqueous solutions, Spectrochim. Acta - Part A Mol. Biomol. Spectrosc. 55 (1999) 1395–1405, https://doi.org/10.1016/S1386-1425(98)00303-5.

[52] I.A. Fisher, A.T. Bell, A mechanistic study of methanol decomposition over Cu/SiO_2, ZrO_2/SiO_2, and Cu/ZrO_2/SiO_2, J. Catal. 184 (1999) 357–376, https://doi.org/10.1006/jcat.1999.2420.

[53] S. Trautmann, M. Baerns, Infrared Spectroscopic Studies of CO Adsorption on Rhodium Supported by SiO_2, Al_2O_3, and TiO_2, J. Catal. 150 (1994) 335–344, https://doi.org/10.1006/jcat.1994.1352.

[54] J.-D. Grunwaldt, L. Basini, B.S. Clausen, In Situ EXAFS Study of Rh/Al_2O_3 Catalysts for Catalytic Partial Oxidation of Methane, J. Catal. 200 (2001) 321–329, https://doi.org/10.1006/jcat.2001.3211.

[55] S.M. McClure, M.J. Lundwall, D.W. Goodman, Planar oxide supported rhodium nanoparticles as model catalysts, Proc. Natl. Acad. Sci. U. S. A. 108 (2011) 931–936, https://doi.org/10.1073/pnas.1006635107.

[56] W.M.H. Sachtler, M. Ichikawa, Catalytic site requirements for elementary steps in syngas conversion to oxygenates over promoted rhodium, J. Phys. Chem. 90 (1986) 4752–4758, https://doi.org/10.1021/j100411a009.

[57] R.P. Underwood, A.T. Bell, Lanthana-promoted Rh/SiO_2. I. Studies of CO and H_2 adsorption and desorption, J. Catal. 109 (1987) 61–75. https://doi.org/10.1016/0021-9517(88)90185-6.

[58] B.T. Loveless, C. Buda, M. Neurock, E. Iglesia, CO Chemisorption and Dissociation at High Coverages during CO Hydrogenation on Ru Catalysts, J. Am. Chem. Soc. 135 (2013) 6107–6121, https://doi.org/10.1021/ja311848e.

[59] B. Sen, J.L. Falconer, Detection of activated adsorption sites and a CO-H surface complex on Ru/Al_2O_3, J. Catal. 113 (1988) 444–452, https://doi.org/10.1016/0021-9517(88)90270-9.

[60] P.G. Glugla, K.M. Bailey, J.L. Falconer, Isotopic Identification of Surface Site Transfer on Ni/Al_2O_3 Catalysts, J. Phys. Chem. 92 (1988) 4474–4478, https://doi.org/10.1021/j100326a045.

[61] P.G. Glugla, K.M. Bailey, J.L. Falconer, Activated formation of a H-CO complex on Ni/Al_2O_3 catalysts, J. Catal. 115 (1989) 24–33, https://doi.org/10.1016/0021-9517(89)90004-3.

[62] B. Sen, J.L. Falconer, Site transfer and a support-bound -HCO Complex on Ni/TiO_2, J. Catal. 122 (1990) 68–79, https://doi.org/10.1016/0021-9517(90)90262-I.

[63] J.S. Rieck, A.T. Bell, Studies of the interactions of H_2 and CO with silica- and lanthana-supported palladium, J. Catal. 96 (1985) 88–105, https://doi.org/10.1016/0021-9517(85)90363-X.

[64] R. Brito de Barros, A.R. Garcia, L.M. Ilharco, A RAIRS study of the methanol decomposition on oxygen precovered Ru(0001), Surf. Sci. 502–503 (2002) 156–163, https://doi.org/10.1016/S0039-6028(01)01927-6.

[65] G.J. Millar, C.H. Rochester, K.C. Waugh, Infrared study of methyl formate and formaldehyde adsorption on reduced and oxidised silica-supported copper catalysts, J. Chem. Soc. Faraday Trans. 87 (1991) 2785–2793, https://doi.org/10.1039/FT9918702785.

[66] X. Bao, J. Deng, HREELS of Methanol Oxidation on Polycrystalline Silver Spectroscopy Evidence for Adsorbed Intermediates in the Conversion of Methoxide to Formaldehyde and Water, Catal. Lett. 4 (1990) 25–36, https://doi.org/10.1007/BF00764867.

[67] J.E. Demuth, H. Ibach, Observation of a methoxy species on Ni(111) by high-resolution electron energy-loss spectroscopy, Chem. Phys. Lett. 60 (1979) 395–399, https://doi.org/10.1016/0009-2614(79)80596-5.

[68] B.A. Sexton, Surface vibrations of adsorbed intermediates in the reaction of alcohols with Cu(100), Surf. Sci. 88 (2–3) (1979) 299–318, https://doi.org/10.1016/0039-6028(79)90077-3.

[69] T. Feng, J.M. Vohs, Temperature-programmed desorption study of the selective oxidation of alcohols on silica-supported vanadium oxide, J. Phys. Chem. B. 109 (2005) 2120–2127, https://doi.org/10.1021/jp040165k.

[70] D. Degerman, M. Shipilin, P. Lömker, C.M. Goodwin, S.M. Gericke, U. Hejral, J. Gladh, H.-Y. Wang, C. Schlueter, A. Nilsson, P. Amann, Operando Observation of Oxygenated Intermediates during CO Hydrogenation on Rh Single Crystals, J. Am. Chem. Soc. 144 (16) (2022) 7038–7042, https://doi.org/10.1021/jacs.2c00300.